Insights into the role of Ce and Sm in improving low-temperature NH_3-SCR performance over Ce-Sm/Cu-SSZ-13 coupled catalysts

Ruibin Sun[a], Yu Lyu[a,b], Chonglin Song[a,*], Chenxi Wang[a,c], Gang Lyu[a], Xiangyu Dong[a], Lei Tian[a], Xinhui Liu[a], Yibo Xu[a]

[a] State Key Laboratory of Engines, Tianjin University, Tianjin 300072, China

[b] China Automotive Engineering Research Institute Co., Ltd, Chongqing 401122, China

[c] Institute for Transport Studies, University of Leeds, Leeds LS2 9JT, UK

**Corresponding author：Chonglin Song*

Postal address: State Key Laboratory of Engines, Tianjin University, Tianjin 300072, China

E-mail: songchonglin@tju.edu.cn

Abstract

The increasingly stringent requirements for controlling nitrogen oxide (NOx) emissions during the cold start conditions of diesel engines serve as a powerful driving force to enhance the low-temperature NH_3-SCR performance of state-of-the-art commercial Cu-SSZ-13. In this study, the coupled catalysts were synthesized to create additional active sites for NO oxidation and NH_3 adsorption/activation, and the synergistic effect between Cu species and CeO_2/Sm_2O_3 leads to a substantial boost in the low-temperature NH_3-SCR activity of CSZ. The results suggest that 6% Ce-2% Sm/CSZ, as the optimal coupled catalyst, achieves a NOx conversion of 93.1% at 200 ℃, significantly higher than that of CSZ. The coupled CeO_2 and Sm_2O_3 enhance the number of both Brønsted and Lewis acid sites on CSZ, promoting the adsorption and activation of NH_3. Therefore, 6% Ce-2% Sm/CSZ can form more NH_4^+ adsorbed on the Lewis acid sites, which reacts with free ionic nitrates to form NH_4NO_3. More importantly, the coupled Sm_2O_3 facilitates the conversion of NH_4NO_3 by NO to

easily decomposable NH_4NO_2. In addition, additional oxygen vacancies provided by Ce^{3+} can adsorb O_2 and promote the transport of oxygen ions, and electron donation from Sm^{3+} to $[ZCu^{2+}(OH)]^+$ enhances the low-temperature activity of the latter. Ultimately, the low-temperature NH_3-SCR performance of CSZ is improved via a synergistic effect. The NH_3-SCR reaction over 6% Ce-2% Sm/CSZ co-follows the Eley-Rideal (E-R) and Langmuir-Hinshelwood (L-H) mechanisms.

Keywords: low-temperature NH_3-SCR, Cu-SSZ-13, CeO_2, Sm_2O_3, synergistic effect

1. Introduction

Nitrogen oxides (NOx) are thought of as one of the major detrimental atmospheric pollutants which are inextricably linked to a spectrum of serious problems including human health and ecological environment [1–4]. Currently, the measures to reduce NOx from mobile sources are frequently used in conjunction with optimizing combustion systems to decrease NOx formation and implementing high-efficiency exhaust after-treatment technologies to purify NOx [5–8], thereby meeting emission regulations and legislation. Among these technologies, the selective catalytic reduction of NOx by NH_3 (NH_3-SCR) under conditions of excess O_2 has been proved to be one of the most effective and best available methods for decreasing NOx emissions [9,10]. Nowadays, the state-of-the-art commercial Cu-SSZ-13, with chabazite (CHA) structure, has been acknowledged as one of the most prevalently employed catalysts in the NH_3-SCR reaction process, primarily attributing to its outstanding catalytic performance, excellent hydrothermal stability and high N_2 selectivity [11–13]. Actually, Cu-SSZ-13 catalyst still encounters some inevitable problems when applied in the field of denitration. Based on the fact that the light-off temperature of the Cu-SSZ-13 catalyst (i.e., the minimum temperature at which it starts to exert catalytic activity) is typically higher than the exhaust temperature emitted by the engine during the cold start phase, the catalytic performance of the Cu-

SSZ-13 catalyst at low temperatures falls short of meeting the demands of practical applications [14]. Therefore, there is an eager anticipation for the improvement of the Cu-SSZ-13 catalyst, which should be capable of functioning efficiently at low temperatures and possessing a broad operational temperature range.

The general consensus is that Z_2Cu^{2+} located at the 6-membered rings (6MRs) and $[ZCu^{2+}(OH)]^+$ located at the 8-membered rings (8MRs) (Z stands for the framework negative charge) are considered to be the main active sites of SSZ-13 in NH_3-SCR [15,16]. Meanwhile, the $[ZCu^{2+}(OH)]^+$ plays a crucial role in the low-temperature region [9,17]. At present, it has been discovered that introducing a secondary cation can facilitate the exchange of Cu^{2+} onto the sites of SSZ-13, resulting in the formation of a greater number of $[ZCu^{2+}(OH)]^+$ ions. For example, Wang et al. [18] reported that Nb-incorporated Cu-SSZ-13 possesses a larger number of $[ZCu^{2+}(OH)]^+$ which is the active center at low temperature since niobium (Nb) can promote the occupation of Cu^{2+} ions at sites located on the 8MRs of SSZ-13. Lee et al. [19] proposed that Cu^{2+} ions exist more predominantly in the form of $[ZCu^{2+}(OH)]^+$ ions compared to Z_2Cu^{2+} ions due to the fact that pre-loaded Co^{2+} ions have a tendency to preferentially occupy the sites in 6MRs. Despite the fact that introducing a secondary cation to increase the number of $[ZCu^{2+}(OH)]^+$ ions represents an effective means of enhancing the activity of Cu-SSZ-13 under low-temperature conditions, the number of exchangeable sites in SSZ-13 is finite. Researchers have been persistently exploring more efficient and practical methods with the aim of markedly enhancing the activity of catalysts in low-temperature environments.

In 1994, a “metal oxide + zeolite” coupled catalyst for HC-SCR reactions was successfully synthesized by Yokoyama et al [20]. They utilized a mechanical mixing technique to combine Ce/ZSM-5 with Mn_2O_3 or CeO_2, achieving a significant improvement in the denitrification efficiency

of Ce/ZSM-5 at low temperatures. Since then, a substantial amount of composite or coupled catalysts have undergone extensive and profound investigation. Huang et al [21] demonstrated that the low-temperature NH_3-SCR performance of Cu-SSZ-13 was directly affected by oxygen species derived from metal oxides, including CeOx, ZrOx and MnOx. MnOx with abundant chemisorbed oxygen promoted the formation of highly active bridging nitrate species, whereas CeOx and ZrOx with abundant lattice oxygen tended to form less reactive bidentate and monodentate nitrate species. Kim et al [22] successfully prepared a dual-functional hybrid catalyst and clearly pointed out that improved low-temperature performance was attributed to the fact that the zeolite promoted the decomposition of nitrate derived from MnOx. Xu et al. [23] reported that unstable intermediate HONO species were formed on the solid solution (CeZrOx) during NO oxidation and migrated to the active component (Cu-SSZ-13) reacting with NH_3 adsorbed on the Brønsted acid sites to produce NH_4NO_2. Kim et al [24] designed an ingenious hybrid catalyst system in which the activated NO intermediates generated over MnOx migrated to the Brønsted acid sites of the H-Y zeolite. This hybrid catalyst exhibited excellent low-temperature activity. Based on the above analysis, it was found that the highly active intermediates were formed on the metal oxides and subsequently migrated to zeolites for decomposition or reaction.

Typically, other metals are introduced into Cu-SSZ-13 to enhance its performance. For instance, CeO_2 has been subject to extensive and in-depth research in the NH_3-SCR reaction since it can provide wonderful oxygen storage and release capacity to adjust the concentration of oxygen in the exhaust gas and unexceptionable redox properties connected with the valence state transition capability between Ce^{3+} and Ce^{4+}, thereby promoting the elimination of NOx. However, it also has some drawbacks. The catalytic activity of Ce-modified Cu-SSZ-13 may be insufficient under low-

temperature conditions (≤250 ℃), which further restricts its application during the cold-start phase of diesel engines [25,26]. Recently, the introduction of an appropriate amount of Sm into MnOx, CeO_2-MnOx and/or MnOx-TiO_2 could effectively promote the formation of Mn^{4+} and chemically adsorbed oxygen, thereby enhancing their low-temperature NH_3-SCR performance [27–29]. However, there are limited research reports available on the development of coupled catalysts incorporating metal oxides (CeO_2 and SmO_2) with Cu-SSZ-13 for enhancing low-temperature NH_3-SCR performance. In addition, a definitive explanation for the detailed synergistic mechanisms between zeolites and metal oxides in coupled catalysts has not been fully established. Therefore, in this study, the combination of rare earth oxides (CeO_2 and/or Sm_2O_3) with commercial Cu-SSZ-13 aims to obtain coupled catalysts (6% CeO_2-2% Sm_2O_3/Cu-SSZ-13, indicated as 6% Ce-2% Sm/CSZ) by the slurry method to markedly enhance the low-temperature performance of CSZ at 200 ℃. More importantly, the synergy mechanism of 6% Ce-2% Sm/CSZ coupled catalyst is more thoroughly explored and unveiled by employing advanced technology.

2. Experiment and Method

2.1 Preparation of coupled catalysts

The coupled catalysts were successfully synthesized. The Cu-SSZ-13 (Zhuoran Environmental Protection Co., Ltd) with a pore size of 0.3 ~ 0.4 nm and SiO_2/Al_2O_3 molar ratio of 20 was purchased and the Cu content in Cu-SSZ-13 accounted for 4.12 wt%. A specific quantity of silica sol (Zhengzhou Xinpei Chemical products Co., Ltd) + aluminum sol (Dezhou Keying New Material Co., Ltd) as well as cellulose (Macklin, ≥ 95.0%) was utilized as complexing agent and dispersing agent, respectively. The slurry was formulated with Cu-SSZ-13 (32 wt%), binder (3 wt%), cellulose (1 wt%) and deionized water (64 wt%). Subsequently, an appropriate amount of CeO_2 (Macklin, ≥ 99.9%) or CeO_2 + Sm_2O_3

(Macklin, ≥ 99.9%) was introduced into the slurry, respectively. Among them, the Ce/Sm element contents and Cu-SSZ-13 contents in the slurry were maintained at 32 wt%. A 300 cpsi honeycomb cordierite monolith (CC, Shandong Aofu Environmental Protection Technology Co, Ltd) with 30 mm length, 20 mm diameter and 0.18 mm wall thickness was put into the slurry. The surplus slurry inside the straight track was cleared away by compressed air, effectively preventing any blockage of the channel. The prepared catalysts were dried at 120 ℃ for 12 h and calcined at 550 ℃ for 4 h to obtain the final coupled catalysts. The desired coating loading of 36 wt% was deposited onto CC. As a comparison, the slurry containing only Cu-SSZ-13 was designated as CSZ. In addition, the Ce element contents in Ce/CSZ of 5, 6, 7, 8 and 10 wt%, and second promoting metal Sm element contents in Ce-Sm/CSZ of 1, 2 and 3 wt% were employed in this study. The obtained coupled catalysts were labeled as *x*% Ce-*y*% Sm/CSZ, where *x* and *y* represented the weight contents of the Ce and Sm elements, respectively. In addition, the actual contents of Cu, Sm, and Ce in the coupled catalysts were measured by ICP-OES, and the results are presented in Table 1.

Table 1 Actual contents of Cu, Ce, and Sm in the coupled catalysts

Coupled catalysts	Cu (wt%)	Ce (wt%)	Sm (wt%)
CSZ	3.45	–	–
6% Ce/CSZ	3.24	6.02	–
8% Ce/CSZ	3.15	7.93	–
10% Ce/CSZ	2.96	10.17	–
6% Ce-2% Sm/CSZ	3.12	5.91	1.97

2.2. Characterization of coupled catalysts

The elemental contents of Cu, Ce and Sm, crystal structure, texture properties and element

distribution of the coupled catalysts were investigated by means of inductively coupled plasma-optical emission spectrometry (ICP-OES), X-ray diffraction (XRD), scanning electron microscope (SEM) and energy dispersive spectrometer (EDS). For the analysis of Cu species in the coupled catalysts, the redox properties and electrostatic interactions were examined through the application of H_2 temperature-programmed reduction (H_2-TPR) and X-ray photoelectron spectra (XPS) techniques. The adsorption and desorption behaviors of NOx and NH_3 on the coupled catalysts were tested by NH_3/($NO+O_2$)-temperature-programmed desorption (NH_3/($NO+O_2$)-TPD) and in situ diffuse reflectance infrared fourier transform spectroscopy (In situ DRIFTS). In addition, the comprehensive experimental procedures have been outlined in the Supplementary data.

2.3. NH_3-SCR steady-state reaction experiments

The NH_3-SCR steady-state reaction experiments were carried out in a fixed-bed continuous flow quartz reactor with an inner diameter of 20 mm at atmospheric pressure. The desired reaction temperature and flow rate were regulated and controlled by the furnace with PID control and the mass flow controller, respectively. The gas hourly space velocity (GHSV) of the reaction feed gas was 70,000 h^{-1} (total flow rate of 8.110 L min^{-1}), with a composition comprising 1100 ppm NH_3, 1000 ppm NO, 10 vol% O_2, 5 vol% water vapour (only used for the water vapour tolerance research) and argon (Ar) as the balance gas. To assess the influence of thermal aging on the performance of the coupled catalysts, the coupled catalysts were subjected to a thermal treatment at 800°C for 4 h. The steady-state outlet concentrations of NO_2, N_2O, NH_3 and NO during the NH_3-SCR reaction were tracked using an online mass spectrometer manufactured by V&F corporation from Austria. The essential parameters for assessing the catalytic performance of the coupled catalysts were expressed through equations (1) and (2):

$$\text{NOx conversion} = \frac{C_{\text{NO,in}} - C_{\text{NO,out}}}{C_{\text{NO,in}}} \times 100\% \quad (1)$$

$$\text{N}_2 \text{ selectivity} = 1 - \frac{2C_{\text{N}_2\text{O,out}} + C_{\text{NO}_2\text{,out}}}{C_{\text{NO,in}} - C_{\text{NO,out}} + C_{\text{NH}_3\text{,in}} - C_{\text{NH}_3\text{,out}}} \times 100\% \quad (2)$$

where the $C_{g,in}$ and $C_{g,out}$ denote feed and effluent gases concentration of species g.

3. Results and Discussion

3.1 NH_3-SCR catalytic performance

NH_3-SCR steady-state performance of the coupled catalysts was tested, as depicted in Fig. 1 and Fig. S1. The optimal catalytic performance of CSZ is observed between 250 and 450 ℃ (Fig. 1a). However, CSZ demonstrates poor catalytic performance at 200 ℃ (69.2%) and 225 ℃ (83.3%). After coupled CeO_2, the coupled catalysts outperform CSZ in catalytic performance. 8% Ce/CSZ possesses higher catalytic performance at 219–405 ℃ (NOx conversion above 95%) and achieves nearly 100% NOx conversion at 250–350 ℃. In particular, the NOx conversion on 8% Ce/CSZ (83.4%) is 14.2% higher than that on CSZ (69.2%) at 200 ℃. After coupled CeO_2 and Sm_2O_3, the NOx conversion of *x*% Ce-*y*% Sm/CSZ shows a similar trend across the reaction temperature window (Fig. S1a), and the 6% Ce-2% Sm/CSZ demonstrates the optimal catalytic performance among *x*% Ce-*y*% Sm/CSZ. Furthermore, the NH_3-SCR performance of 6% Ce-2% Sm/CSZ surpasses that of CSZ and 8% Ce/CSZ, particularly evident in its NOx conversion exceeding 90% within 190–550 ℃. What's more, a NOx conversion of 93.1% is achieved over 6% Ce-2% Sm/CSZ at 200 ℃. These results can indicate that a synergistic effect exists between Ce and Sm to promote low-temperature NH_3-SCR. As shown in Fig. S1b, for CSZ, 8% Ce/CSZ and 6% Ce-2% Sm/CSZ, no N_2O products are detected when the reaction temperature is less than 250 ℃. However, the N_2O product is detected at reaction temperatures above 250 ℃. It is notable that the N_2O concentration in the 6% Ce-2% Sm/CSZ remains below 10 ppm for

the duration of the reaction. In addition, all the catalysts display a N_2 selectivity of more than 93% (Fig. 1b).

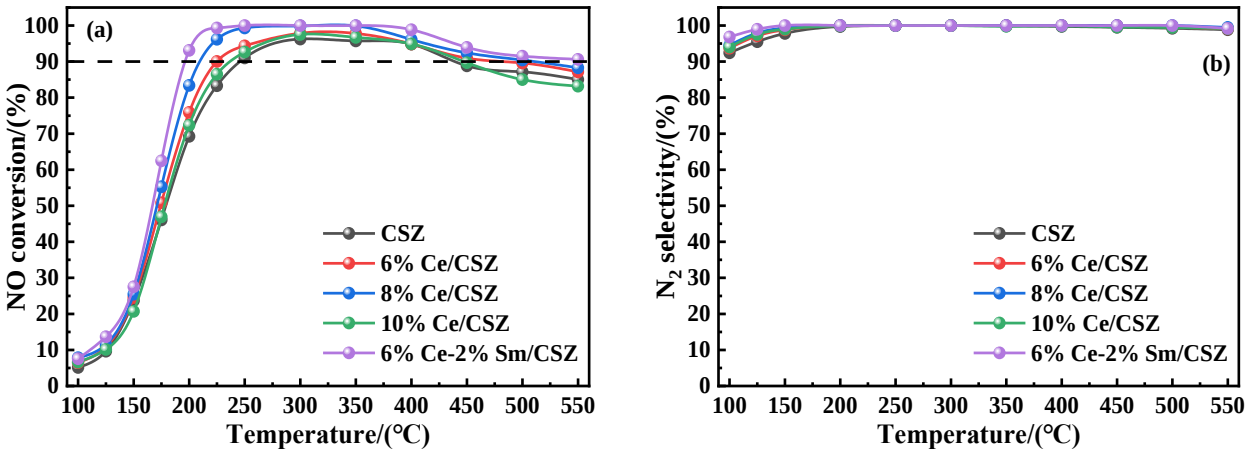

Fig. 1. (a) NOx conversion and (b) N_2 selectivity of the coupled catalysts.

Fig. S2a displays the NH_3-SCR performance of the coupled catalysts in the presence of 5 vol% water vapour. There is a slight increase in NH_3-SCR performance for coupled catalysts across the temperature range of 100–550 ℃. Fig. 2a shows the NOx conversion of the coupled catalysts as a function of time at 200 ℃ under 5 vol% water vapor conditions. An increase in NOx conversion is observed for CSZ, 8% Ce/CSZ and 6% Ce-2% Sm/CSZ (from 100 to 400 min). For instance, the NOx conversion enhances gradually from 83.9 to 87.6% for 8% Ce/CSZ and from 93.1 to 97.7% for 6% Ce-2% Sm/CSZ (from 100 to 180 min). It has been reported that water vapour significantly reduces the reaction energy barrier between $[Cu^{I}(NH_3)_2]^+$ and $[Cu^{II}(NH_3)_2]^{2+}$ [30,31]. Another viewpoint holds that NH_3 adsorbed on Brønsted acid sites can diffuse to Lewis acid sites because hydrogen bonds are formed by adsorbed NH_3 and water vapour [32,33]. Consequently, an enhancement in catalytic activity is achieved. Full recovery of NO conversion can be achieved by removing water vapour from the reaction atmosphere, which indicates that the change in catalytic performance of the coupled catalysts induced by water vapour is reversible.

NOx conversion reduces to different extents in coupled catalysts after thermal aging treatment at 800 ℃ for 4 h, but the use of coupled CeO_2 and/or Sm_2O_3 can effectually alleviate the loss of NOx conversion in CSZ (Fig. 2b), particularly at reaction temperatures ranging from 175 to 300 ℃. Consistent NOx conversion above 80% is maintained on CSZ in the temperature range of 247 to 550 ℃, while more than 80% NOx conversion on 6% Ce-2% Sm/CSZ and 8% Ce/CSZ is achieved at 193–550 ℃ and 223–550 ℃, respectively. These results indicate that coupled Ce and/or Sm can broaden the reaction window of low-temperature NH_3-SCR. As shown in Fig. S2, the N_2 selectivity of the coupled catalysts after thermal aging slightly decreases compared to that of the fresh coupled catalysts. After thermal aging, it is noteworthy that the N_2 selectivity of 6% Ce-2% Sm/CSZ is superior to that of CSZ and 8% Ce/CSZ. For instance, the N_2 selectivity of CSZ and 8% Ce/CSZ exceeds 98% in the temperature ranges of 197–372 ℃ and 188–471 ℃, respectively. In contrast, the N_2 selectivity of 6% Ce-2% Sm/CSZ remains above 98% over a significantly wider temperature range of 125–550 ℃.

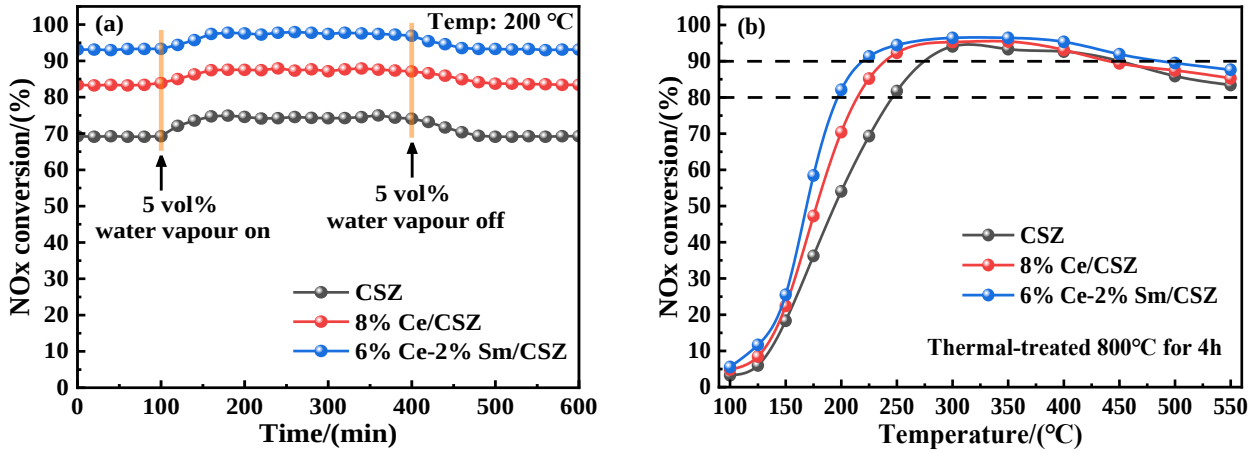

Fig. 2. NOx conversion of CSZ, 8% Ce/CSZ and 6% Ce-2% Sm/CSZ (a) in the presence of 5 vol% water vapour at 200 ℃ and (b) after thermal aging treatment at 800 ℃ for 4 h.

3.2 Textural properties

XRD was employed to detect the crystal structure and phase composition of the coupled catalysts, and the results are displayed in Fig. 3. The major characteristic diffraction peaks located at 2θ = 9.5°,

12.9°, 14.1°, 16.0°, 17.8°, 20.6°, 25.1° and 30.6° are accurately associated with the internal crystal structure of SSZ-13 (PDF# 47–0762), which demonstrates that all the coupled catalysts continue to retain the typical CHA structure after coupled CeO_2 and CeO_2-Sm_2O_3. There are not any characteristic diffraction peaks identified as associated with Cu species or Sm_2O_3, indicating that the Cu species are very well incorporated onto the active sites within the SSZ-13 framework and the Sm_2O_3 species are extremely uniformly distributed on the surface of SSZ-13 or the introduced Sm_2O_3 species are in the nanoscale size. After coupled CeO_2, a more noteworthy phenomenon is that the characteristic diffraction peaks attributed to CeO_2 are detected at 2θ angles of 28.5°(1,1,1), 33.0°(2,0,0), 47.3°(2,2,0), 56.3°(3,1,1) and 59.0°(2,2,2), which correspond to CeO_2 with a cubic crystal structure (PDF# 43-1002).

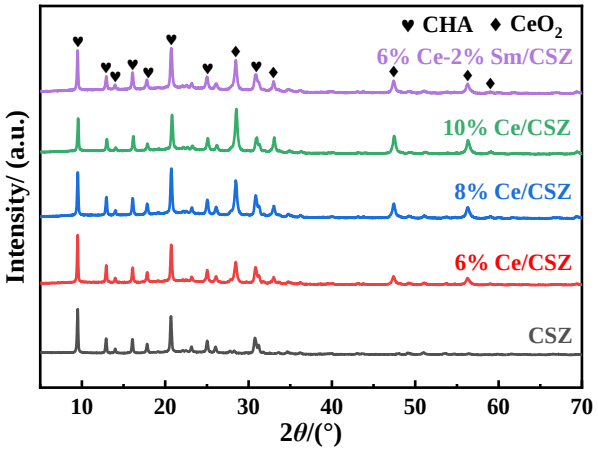

Fig. 3. XRD patterns of CSZ and the coupled catalysts.

For the purpose of conducting a more in-depth observation and analysis of the morphological changes and elemental distribution in the coupled catalysts, SEM and EDS imaging were performed on Cu-SSZ-13, *x*% Ce/CSZ (*x* = 6, 8 and 10) and 6% Ce-2% Sm/CSZ, as demonstrated in Fig. 4 and Fig. S3. Cu-SSZ-13 displays cubic crystals with sizes ranging from 0.25 to 0.30 μm (Fig. 4) and exhibits a uniform distribution of Cu, Si, Al and O elements (Fig. S3). The morphologies of CSZ, *x*% Ce/CSZ (*x* = 6 and 8) and 6% Ce-2% Sm/CSZ show similarities to those of Cu-SSZ-13, and the CeO_2 and/or Sm_2O_3 species exhibit a uniform distribution on the surface of CSZ with cubic crystals, as

verified by the SEM and EDS data in Fig. 4 and Fig. S3. Severe agglomeration is observed in the 10% Ce/CSZ. Additionally, the XRD analysis reveals that the intensities of the characteristic diffraction peaks at 2θ = 9.5° and 20.6° are slightly lower than those of CSZ and the ICP-OES results indicate that the actual Cu content (2.96 wt%) is slightly lower than the nominal Cu content (3.11 wt%). According to the changes in the intensities of the characteristic diffraction peaks and the actual Cu content, it can be inferred that excess CeO_2 covers part of the SSZ-13 framework structure. This result could be one of the factors contributing to the reduced catalytic activity of 10% Ce/CSZ coupled catalyst.

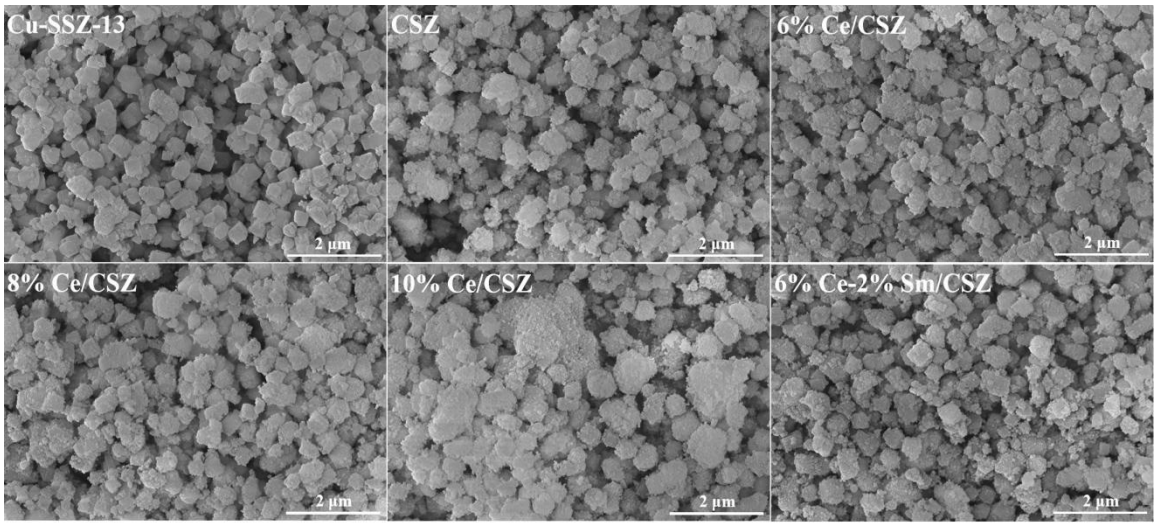

Fig. 4. SEM images of Cu-SSZ-13 and the coupled catalysts.

3.3 Active species

To explore the effects of CeO_2 and/or Sm_2O_3 on the catalytic activity of the coupled catalysts, the reduction properties of Cu species in the coupled catalysts were studied by using H_2-TPR. As illustrated in Fig. 5a, the reduction peaks are detected at approximately 220, 297, 380 and 445 ℃, corresponding to the reduction of $[ZCu^{2+}(OH)]^+$ to Cu^+, CuO to Cu^0, Z_2Cu^{2+} to Cu^+ and Cu^+ to Cu^0, respectively [23,34–36]. The reduction peak temperature of the *x*% Ce/CSZ does not change

232 significantly compared to CSZ. It demonstrates that the reduction properties of Cu species remain
233 unaffected by the presence of CeO_2. In addition, $[ZCu^{2+}(OH)]^+$ and Z_2Cu^{2+}, as the most important
234 catalytically active sites, exhibit significantly different effects on catalytic performance during the
235 NH_3-SCR reaction [18,34]. Nevertheless, $[ZCu^{2+}(OH)]^+$ serves as the catalytically active sites at low
236 temperatures [9,17]. Compared with CSZ and 8% Ce/CSZ, the reduction peak temperature of
237 $[ZCu^{2+}(OH)]^+$ in 6% Ce-2% Sm/CSZ shifts toward lower temperatures by 10 and 9 ℃, respectively,
238 which suggests that Sm species can enhance the reduction property of $[ZCu^{2+}(OH)]^+$. Tong et al. [37]
239 pointed out that Sm species can modulate the reduction property of active components. Therefore, 6%
240 Ce-2% Sm/CSZ displays the best catalytic performance. In addition, the concentration of
241 $[ZCu^{2+}(OH)]^+$ in the coupled catalysts reduced by H_2 was calculated and summarized in Table 2. The
242 H_2 consumption of 85.01 μmol g^{-1} is observed for $[ZCu^{2+}(OH)]^+$ on CSZ. After coupled CeO_2 and/or
243 Sm_2O_3, the gradual decrease in H_2 consumption of $[ZCu^{2+}(OH)]^+$ on the coupled catalysts is attributed
244 to the reduced proportion of CSZ in the coupled catalysts. The H_2 consumption of $[ZCu^{2+}(OH)]^+$ in 8%
245 Ce/CSZ and 6% Ce-2% Sm/CSZ is remarkably similar, at approximately 77.58 μmol g^{-1}, indicating
246 that the concentration of $[ZCu^{2+}(OH)]^+$ is not influenced by CeO_2 and CeO_2-Sm_2O_3. Unexpectedly,
247 the opposite experimental phenomenon was discovered. Xu et al. [23] pointed out that CeZrOx
248 enhanced the concentration of $[ZCu^{2+}(OH)]^+$ in CeZrOx-Cu/SSZ-13. Actually, the concentration of
249 $[ZCu^{2+}(OH)]^+$ may be influenced by preparation conditions, such as the pH and particle size of the
250 slurry, the selection and dosage of binders, the Si/Al molar ratio and Cu content in SSZ-13 and other
251 factors. In addition, the catalytic performance of 8% Ce/CSZ and 6% Ce-2% Sm/CSZ at low
252 temperatures is superior to that of CSZ, which further demonstrates the synergistic effect between rare
253 earth oxides (CeO_2 and/or Sm_2O_3 species) and $[ZCu^{2+}(OH)]^+$ ions. Interestingly, the improvement of

254 catalytic activity in CSZ achieved by combining CeO_2 and Sm_2O_3 is greater than that achieved by
255 CeO_2 alone, indicating the differing contributions of CeO_2 and Sm_2O_3 to the NH_3-SCR reaction.

256 The information about surface component and oxidation states in the coupled catalysts needs to
257 be investigated. Therefore, XPS characterization was performed. The coupled catalysts' Cu 2p, O 1s,
258 Ce 3d and Sm 3d spectra are illustrated in Fig. 5b-e, and the surface $Cu^{2+}/(Cu^{2+} + CuO)$ concentration
259 and peak area proportion (O_{ads} and Ce^{3+}) are presented in Table 2. Fig. 5b illustrates that the spin-orbit
260 splitting results in two distinct Cu 2p peaks located at approximately 932.6 eV (Cu $2p_{3/2}$) and 953.1
261 eV (Cu $2p_{1/2}$), respectively [25,38,39]. Additionally, the shake-up satellite of Cu is detected at around
262 944.1 eV, which suggests that the Cu species in the coupled catalysts mainly exist in the form of + 2
263 [40,41]. The Cu $2p_{3/2}$ peak can be split into two peaks presenting at approximately 933.2 eV (CuO
264 species) and 936.6 eV (Cu^{2+}) [36,42]. After coupled CeO_2, the binding energy (at approximately 936.6
265 eV) of Cu^{2+} and the surface $Cu^{2+}/(Cu^{2+} + CuO)$ concentration (at approximately 15 at%) in CSZ and
266 *x*% Ce/CSZ (*x* = 6 and 8) remain almost unchanged (Fig. 5b and Table 2), indicating that CeO_2 does
267 not affect the characteristics of Cu^{2+} species. However, compared with CSZ and 8% Ce/CSZ, the
268 binding energy of Cu^{2+} in 6% Ce-2% Sm/CSZ shifts toward lower binding energy by 0.7 and 0.6 eV,
269 respectively. This result further confirms electron transfer between Sm^{3+} and $[ZCu^{2+}(OH)]^+$. In
270 addition, $[ZCu^{2+}(OH)]^+$ serves as the active sites under low-temperature conditions. Chen et al. [9]
271 pointed out that the activity of $[ZCu^{2+}(OH)]^+$ is enhanced because Sm^{3+} can transfer electrons to
272 $[ZCu^{2+}(OH)]^+$, which leads to better performance in the low-temperature NH_3-SCR reaction.

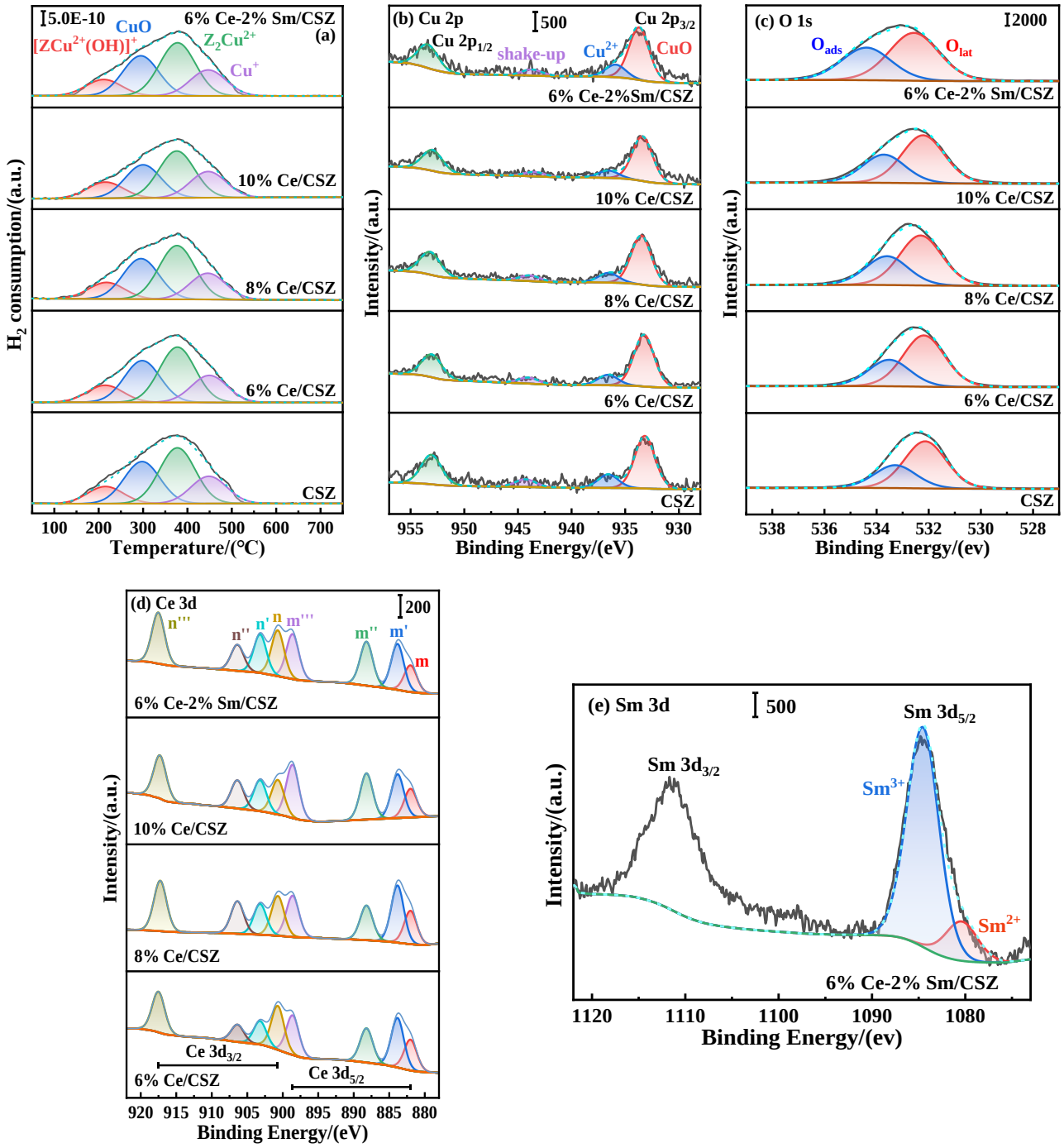

Fig. 5. (a) H_2-TPR, (b) Cu 2p, (c) O 1s, (d) Ce 3d and (e) Sm 3d spectra of the coupled catalysts.

The coupled catalysts' O 1s spectra illustrated in Fig. 5c can be divided into lattice oxygen (O_{lat}) at 532.1–532.6 eV and chemisorption oxygen (O_{ads}) at 533.2–534.4 eV [9,18]. Compared with CSZ, the O 1s peaks for *x*% Ce/CSZ remain virtually unchanged, which suggests that the oxygen species derived from Ce species demonstrate negligible interaction with Cu^{2+} ($[ZCu^{2+}(OH)]^+$ or Z_2Cu^{2+}). It

can be clearly observed from Table 2 that the corresponding peak area proportion of $O_{ads}/(O_{lat} + O_{ads})$ in 6% Ce/CSZ (35.08%), 8% Ce/CSZ (41.61%), 10% Ce/CSZ (33.17%) and 6% Ce-2% Sm/CSZ (43.79%) is higher than that in CSZ (30.67%). It should be pointed out that O_{ads}, as the most active oxygen species, can directly affect redox reactions [43]. After coupled Sm_2O_3, the binding energy of O_{lat} and O_{ads} in 6% Ce-2% Sm/CSZ shifts to higher binding energy, indicating that there exist strong interactions between oxygen species originated from Sm species and Cu^{2+} [9,44]. In addition, the corresponding peak area proportion of $O_{ads}/(O_{lat} + O_{ads})$ in 6% Ce-2% Sm/CSZ is significantly higher than that in CSZ and 8% Ce/CSZ. Therefore, it can be inferred that O_{ads} consists of chemisorption oxygen and hydroxyl group. The additional Brønsted acid sites provided by the hydroxyl group can serve as active centers for NH_3 adsorption and activation [45]. Thus, 6% Ce-2% Sm/CSZ exhibits the best low-temperature activity.

The coupled catalysts' Ce 3d and Sm 3d spectra are illustrated in Fig. 5d and e. It can be seen from Fig. 5d that the peaks denoted as m (~ 882.0 eV), m' (~ 883.8 eV), m'' (~ 888.2 eV) and m''' (~ 898.6 eV) are deemed to be Ce $3d_{5/2}$, and the peaks marked as n (~ 900.7 eV), n' (~ 903.2 eV), n'' (~ 906.4 eV) and n''' (~ 917.3 eV) are considered to be Ce $3d_{3/2}$, respectively [46,47]. In addition, m' and n' peaks are designated as Ce^{3+}, and the other peaks are assigned as Ce^{4+}. The corresponding peak area proportion of $Ce^{3+}/(Ce^{3+} + Ce^{4+})$ in 6% Ce/CSZ and 6% Ce-2% Sm/CSZ is 24.13 and 24.63% (Table 2), respectively. It enhances slightly after coupled Sm_2O_3, so it can be inferred that Sm species can improve the formation of Ce^{3+} to a certain extent. It has been reported that the additional oxygen vacancies provided by Ce^{3+} can effectively adsorb O_2 in the gas phase and promote the transport of oxygen ions in the coupled catalysts [48,49]. In brief, it can improve catalytic activity at low temperatures. This result indicates that a synergistic interaction exists among Ce, Sm and Cu species.

According to Fig. 5e, the peaks at around 1111.3 and 1084.4 eV of the Sm 3d are ascribed to Sm $3d_{3/2}$ and Sm $3d_{5/2}$, respectively. The Sm $3d_{5/2}$ peaks can be split into two peaks, i.e., one peak at around 1080.4 eV corresponds to Sm^{2+}, and the other peak at around 1084.5 eV corresponds to Sm^{3+} [50,51], which suggests that Sm exists primarily in the form of + 3 in 6% Ce-2% Sm/CSZ.

Table 2 Changes in the content of Cu species and in the relative area proportion of O_{ads} and Ce^{3+} over the coupled catalysts.

Coupled catalysts	[a] H_2 consumption (μmol g^{-1})			[b] Surface $Cu^{2+}/(Cu^{2+}+CuO)$ concentration (at%)	[b] $O_{ads}/(O_{ads}+O_{lat})$ (%)	[b] $Ce^{3+}/(Ce^{3+}+Ce^{4+})$ (%)
	$[ZCu^{2+}(OH)]^+$	Z_2Cu^{2+}	Total			
CSZ	85.01	191.40	276.41	16.47	30.67	—
6% Ce/CSZ	79.18	178.28	257.46	14.23	35.08	24.13
8% Ce/CSZ	77.69	174.93	252.62	15.45	41.61	27.81
10% Ce/CSZ	65.35	147.11	212.46	9.39	33.17	21.25
6% Ce-2% Sm/CSZ	77.47	174.38	251.85	16.13	43.79	24.63

[a] Analyzed by H_2-TPR. [b] Analyzed by XPS.

3.4 Adsorption/Desorption and activation of $NO+O_2$

3.4.1. $NO+O_2$ adsorption

NOx adsorption plays a particularly critical role in the coupled catalysts, given that NOx is one of the principal reactants in the NH_3-SCR reaction. Therefore, in situ DRIFTS was used to study the adsorbed NOx species on the coupled catalyst during the NOx absorption process at 50 °C, and the results are presented in Fig. 6. Symmetric vibrations of monodentate nitrates (1331 cm^{-1}), free ionic nitrates (1372 cm^{-1}), asymmetric vibrations of monodentate nitrates (1424 cm^{-1}), chelating bidentate nitrates (1615 cm^{-1}), bridging nitrates (1429 cm^{-1}) and absorbed N_2O_4 (1730 cm^{-1}) are observed on

CSZ [52–55], and the peak intensity of adsorbed NOx species gradually enhances with adsorption time from 1 to 10 min. After coupled CeO_2, the peak intensity of adsorbed NOx species on both 6% Ce/CSZ and 8% Ce/CSZ is consistently lower than that on CSZ at any given time point (Fig. 6a, b and c) due to the fact that the proportion of CSZ in the coupled catalysts decreases, which suggests that the adsorption sites for NOx are exclusively located on Cu species. Furthermore, this is consistent with the adsorbed NOx species on *x*% Ce/CSZ (*x* = 6 and 8) and CSZ, indicating that Ce species do not alter the adsorbed NOx species on the coupled catalysts. After coupled Sm_2O_3, an increase in peak intensity of NOx is detected at 1331, 1615 and 1629 cm^{-1}, while a reduction in peak intensity of NOx is observed at 1372 cm^{-1} compared to CSZ and 8% Ce/CSZ at any given time point. However, an interesting phenomenon is that a new peak at 1472 cm^{-1} is noted for 6% Ce-2% Sm/CSZ (Fig. 6d), which is assigned to absorbed NO_2 [56]. This result demonstrates that the Sm species are able to form a rich diversity of adsorbed NOx species, especially the formation of NO_2 on 6% Ce-2% Sm/CSZ. It is widely known that NO_2 can participate in the reaction between NO and NH_3, that is, the "Fast SCR" reaction. As a consequence, 6% Ce-2% Sm/CSZ exhibits excellent low temperature NH_3-SCR performance.

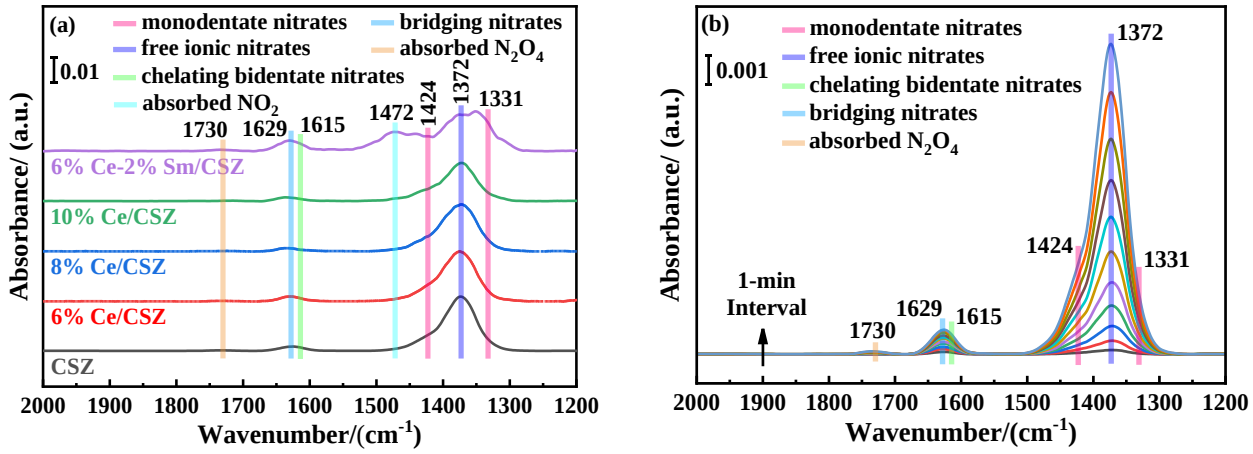

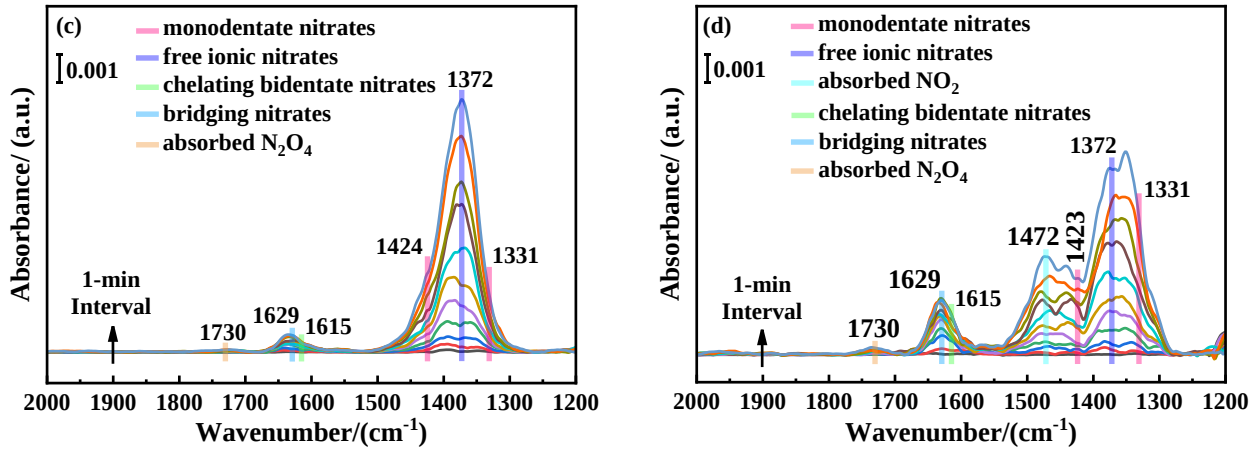

Fig. 6. In situ DRIFTS of NO+O_2 adsorption on: (a) CSZ, *x*% Ce/CSZ and 6% Ce-2% Sm/CSZ at 50 ℃ at 10 min; (b)–(d) Time-dependent profiles for (b) CSZ, (c) 8% Ce/CSZ and (d) 6% Ce-2% Sm/CSZ with exposure durations spanning 1–10 min (at 1 min intervals) at 50 ℃.

3.4.2. NO+O_2 desorption

NO species desorption from the coupled catalysts is displayed in Fig. 7. A shoulder NO desorption peak in the temperature range of 50 to 190 ℃, centered at approximately 122 ℃, can be classified as the decomposition of monodentate nitrates and free ionic nitrates, while another broad and low NO desorption peak in the temperature range of 220 to 450 ℃, centered at around 327 ℃, can be ascribed to the decomposition of bridging nitrates and chelating bidentate nitrates, respectively [27,36,38,57]. After coupled CeO_2 and/or Sm_2O_3, the NO desorption peaks in *x*% Ce/CSZ and 6% Ce-2% Sm/CSZ show almost no change compared to those in CSZ, which suggests that the NO desorption is not affected by Ce and/or Sm species. In addition, it can be seen from Table 3 that the desorption capacities of NOx species on CSZ and 6% Ce/CSZ, 8% Ce/CSZ are 238.61, 214.26 and 188.51 μmol·g^{-1}, respectively. However, the desorption capacity of NOx species on 6% Ce-2% Sm/CSZ closely resembles that on 8% Ce/CSZ. This result reveals that the coupled catalysts exhibit a lower NO desorption capacity compared to CSZ. However, the performance of the coupled catalysts is superior to that of CSZ, which further confirms that there is no significant direct correlation between the

desorption capacity of NO species and the catalytic activity.

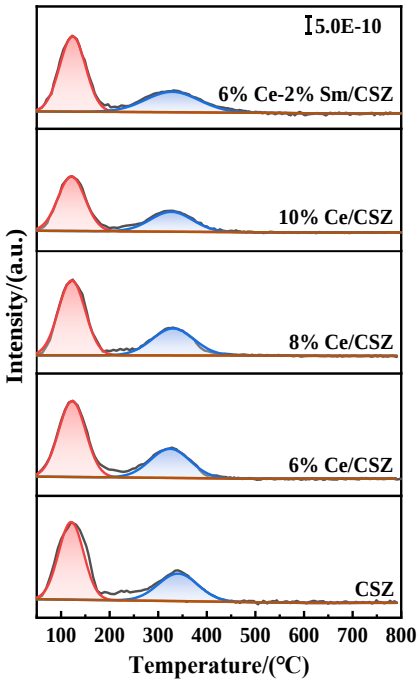

Fig. 7. (NO+O_2)-TPD patterns of the coupled catalysts.

3.5 Acid sites

3.5.1 NH_3 adsorption

The catalytic performance of the coupled catalysts during the NH_3-SCR reaction process is largely governed by the adsorption and activation of NH_3 on adsorption sites (e.g, Brønsted and Lewis acid sites and hydroxyl groups), as displayed in Fig. 8. The peaks located at around 3340, 3267/1454 and 3198 cm^{-1} can be divided into NH_4^+ species adsorbed on Si-OH groups, Lewis acid sites (L-NH_4^+) and Brønsted acid sites (B-NH_4^+), while the peaks centered at approximately 3740/3683/3604 and 1611 cm^{-1} can be classified as NH_3 species adsorbed on Si-OH groups/Al-OH groups/Cu-OH groups and Lewis acid sites (L-NH_3), respectively [18,58–61]. The adsorption sites for NH_3 species on the coupled catalysts do not alter, while the peak intensity for NH_3 species on the coupled catalysts changes relative to CSZ (Fig. 8a), which suggests that the NH_4^+ formation and NH_3 adsorption can be directly affected

by the coupled CeO_2 and/or Sm_2O_3. Therefore, the coupled catalysts exhibit different catalytic activities. Additionally, the temporal evolution of adsorbed NH_3 species over CSZ, 8% Ce/CSZ and 6% Ce-2% Sm/CSZ is monitored via in situ DRIFTS at 50 ℃ (Fig. 8b, c and d). An increase in adsorption time from 1 to 10 min results in a gradual increase in the peak intensity of NH_3 on the catalysts. There are obvious differences in the peak intensity of NH_3 on the catalysts at all times. However, the peak intensity of L-NH_4^+ (3199 cm^{-1}) and L-NH_3 (1609 cm^{-1}) on 6% Ce-2% Sm/CSZ is higher than that on CSZ and 8% Ce/CSZ. The NH_3 and NH_4^+ provided by the Lewis acid sites can act as reactive intermediate species, thereby significantly impacting the low-temperature NH_3-SCR activity of the coupled catalysts [18,62]. Additionally, the formation of B-NH_4^+ on 6% Ce-2% Sm/CSZ is significantly higher than that on CSZ and 8% Ce/CSZ. NH_4^+ provided by the Brønsted acid sites can act as a mobile intermediate in the low-temperature NH_3-SCR reaction [63]. Therefore, the formation of more NH_3 and NH_4^+ on the adsorption sites is more favorable for the low-temperature NH_3-SCR reaction. This is also one of the factors contributing to the optimal catalytic activity of 6% Ce-2% Sm/CSZ.

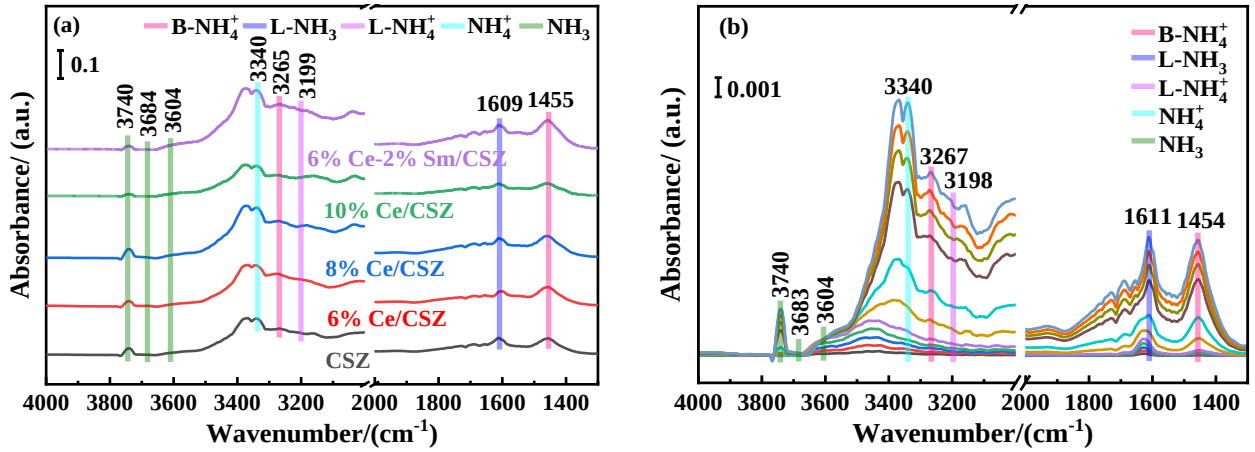

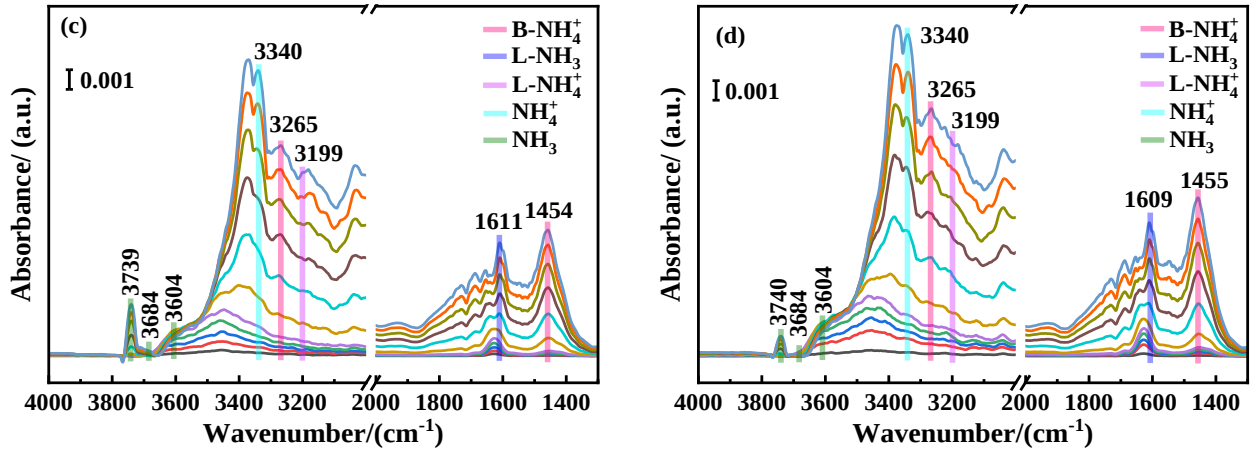

371 Fig. 8. In situ DRIFTS of NH_3 adsorption on: (a) CSZ, *x*% Ce/CSZ and 6% Ce-2% Sm/CSZ at 50 ℃ at 10 min;
372 (b)–(d) Time-dependent profiles for (b) CSZ, (c) 8% Ce/CSZ and (d) 6% Ce-2% Sm/CSZ with exposure durations
373 spanning 1–10 min (at 1 min intervals) at 50 ℃.

374 3.5.2. NH_3 desorption

375 The desorption behavior of NH_3 species and acid content on the coupled catalysts were measured
376 using NH_3-TPD, and the results are displayed in Fig. 9. The desorption peaks of NH_3 species at 178–
377 182 ℃, 326–332 ℃ and 438–443 ℃ can be classified as NH_3 species adsorbed on the weak Lewis
378 acid sites (WLACs), moderate strong Lewis acid sites (MLACs) and Brønsted acid sites (representing
379 the strong acid sites, BACs), respectively [41,64,65]. For all the catalysts, there is no significant
380 difference in the desorption peak temperature of NH_3 species, which suggests that the coupled Ce
381 and/or Sm has no effect on the desorption behavior of NH_3 species at the adsorption sites. The acid
382 content in the coupled catalysts was calculated and summarized in Table 3. The acid content of
383 WLACs, MLACs and BACs on CSZ is only 1.40, 0.37 and 0.10 $mmol \cdot g^{-1}$, respectively, while the acid
384 content of WLACs, MLACs and BACs on 6% Ce-2% Sm/CSZ is 1.99, 0.59 and 0.21 $mmol \cdot g^{-1}$,
385 respectively. This result demonstrates that the coupled Ce and/or Sm primarily enhances the acid
386 amount of WLACs and MLACs. In addition, the additional Lewis acid sites provided by Ce and/or Sm
387 can adsorb more NH_3 species, thereby promoting the low-temperature NH_3-SCR reaction [18,62].

Therefore, the presence of plentiful WLACs and MLACs in 6% Ce-2% Sm/CSZ results in its exceptional low-temperature NH_3-SCR activity.

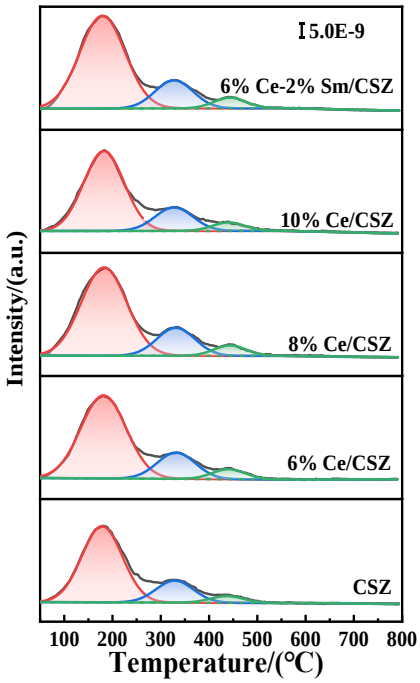

Fig. 9. NH_3-TPD patterns of the coupled catalysts.

Table 3 Changes in the desorption capacity of NOx species and acid content from the coupled catalysts.

Coupled catalysts	[a](NO+O_2)-TPD (μmol·g^{-1})			[b]NH_3-TPD (mmol·g^{-1})			
	50–190 ℃	220–440 ℃	Total	Weak Lewis acid sites (WLACs)	Moderate Lewis acid sites (MLACs)	Brønsted acid sites (BACs)	Total
CSZ	150.35	88.26	238.61	1.40	0.37	0.10	1.87
6% Ce/CSZ	135.59	78.66	214.25	1.78	0.47	0.15	2.40
8% Ce/CSZ	126.13	62.38	188.51	1.92	0.53	0.16	2.61
10% Ce/CSZ	69.35	42.12	111.47	1.53	0.45	0.13	2.11
6% Ce-2% Sm/CSZ	121.25	59.61	180.86	1.99	0.59	0.21	2.79

[a] Analyzed by (NO+O_2)-TPD. [b] Analyzed by NH_3-TPD.

3.6 Reaction route study

3.6.1 Reactions between pre-adsorbed NO + 10% O_2 and NH_3 + 10% O_2

The low-temperature NH_3-SCR reaction route between pre-adsorbed NOx species and NH_3 on 8% Ce/CSZ and 6% Ce-2% Sm/CSZ was investigated using in situ DRIFTS, and the results are displayed in Fig. 10. After exposure to the atmosphere of NH_3 and O_2, throughout the 20-minute monitoring period, no peak related to adsorbed NH_3 species for 8% Ce/CSZ and 6% Ce-2% Sm/CSZ is observed. This finding suggests that pre-adsorbed NOx species can be capable of reacting with gaseous NH_3. For 8% Ce/CSZ and 6% Ce-2% Sm/CSZ, the free ionic nitrates (1372 cm^{-1}) and monodentate nitrates (1423 and 1331 cm^{-1}), as a very important type of reactive intermediates, can participate in low-temperature NH_3-SCR reaction with gaseous NH_3. For 6% Ce-2% Sm/CSZ, an interesting phenomenon is that pre-adsorbed NO_2 (1472 cm^{-1}) can react with gaseous NH_3. It can be inferred that the "Fast SCR" reaction takes place. Consequently, the 6% Ce-2% Sm/CSZ demonstrates improved performance for NH_3-SCR under low-temperature conditions. In brief, pre-adsorbed NOx species on 8% Ce/CSZ and 6% Ce-2% Sm/CSZ react with gaseous NH_3 in the low-temperature NH_3-SCR reaction via the Eley-Rideal (E-R) route.

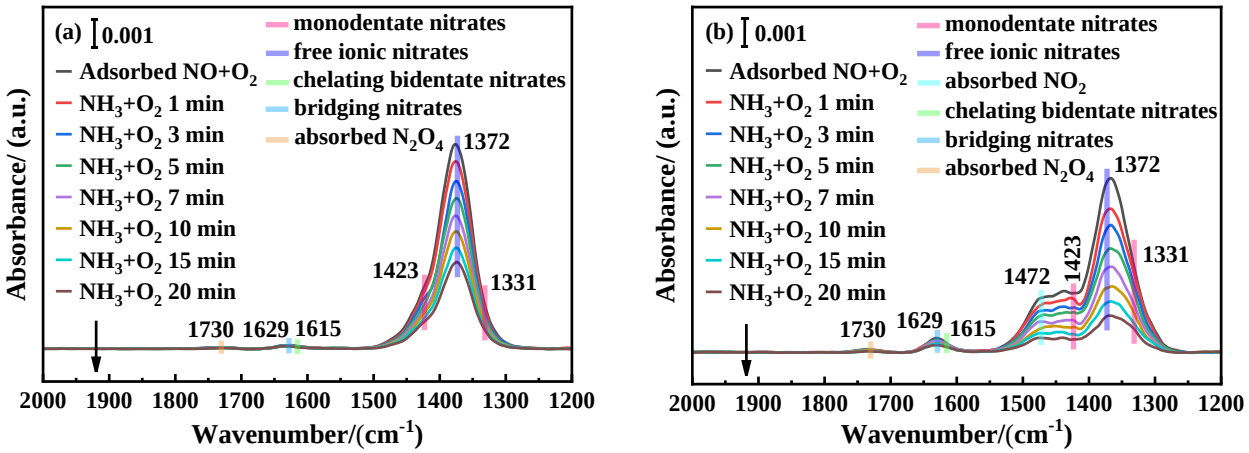

Fig. 10. In situ DRIFTS of pre-adsorbed NO + O_2 followed by reaction with NH_3 + O_2 on (a) 8% Ce/CSZ and (b) 6% Ce-2% Sm/CSZ at 200 ℃.

3.6.2 Reactions between pre-adsorbed NH_3 + 10% O_2 and NO + 10% O_2

The low-temperature NH_3-SCR reaction route between pre-adsorbed NH_3 species and NO on 8%

Ce/CSZ and 6% Ce-2% Sm/CSZ was investigated using in situ DRIFTS, and the results are displayed in Fig. 11. After exposure to the atmosphere of NO and O_2, there exists a significant reduction trend of B-NH_4^+ (1483/1482 and 3265 cm^{-1}), L-NH_3 (1619/1621 cm^{-1}), L-NH_4^+ (3199/3200 cm^{-1}) and NH_4^+ (3340 cm^{-1}) on 8% Ce/CSZ and 6% Ce-2% Sm/CSZ at 200 °C. Lewis acid sites (L-NH_3 and L-NH_4^+) react more rapidly with NOx than Brønsted acid sites (B-NH_4^+). It is well-known that Lewis acid sites are the primary sites for adsorbing and activating NH_3 in low-temperature NH_3-SCR, forming the essential foundation for initiating efficient low-temperature reaction pathways. More importantly, the free ionic nitrates are observed after 15 min on 8% Ce/CSZ and 6% Ce-2% Sm/CSZ. Meanwhile, NH_4NO_3 located at 3057 or 3043 cm^{-1} [36] is detected on 8% Ce/CSZ at 20 min and on 6% Ce-2% Sm/CSZ at 15 min. The formation of NH_4NO_3 may involve the reaction between free ionic nitrates and NH_4^+ originating from Lewis acid sites via the Langmuir-Hinshelwood (L-H) route. Moreover, the NH_4^+ located at the Brønsted acidic sites can migrate to the Lewis acidic sites [63], thus also promoting the formation of NH_4NO_3. Additionally, NH_4NO_3 has been identified as a key intermediate species in the low-temperature NH_3-SCR reaction pathway, while NH_4NO_3 decomposition has been confirmed as a critical step in the mechanism of low-temperature NH_3-SCR. In addition, NH_4NO_3 decomposes via the following pathway: $NH_4NO_3 + NO \rightarrow NH_4NO_2$, and then $NH_4NO_2 \rightarrow N_2 + H_2O$. However, the reaction of NH_4NO_3 with NO proceeds much more slowly [36], and the formation of NH_4NO_3 from the reaction between free ionic nitrates (NO_3^-) and NH_4^+ ($NO_3^- + NH_4^+ \rightarrow NH_4NO_3$) is very fast [36]. When the decomposition of NH_4NO_3 is slower than its formation, NH_4NO_3 may accumulate at the active sites or on the coupled catalyst surface, thereby hindering the progress of the reaction and leading to a decrease in catalytic performance [54,63]. However, the peak intensity of NH_4NO_3 on 6% Ce-2% Sm/CSZ is lower than that on 8% Ce/CSZ, indicating that the coupled Sm_2O_3 can facilitate the

conversion of NH_4NO_3 by NO to NH_4NO_2 [23]. Ultimately, NH_4NO_2, as an extremely unstable intermediate species, easily decomposes into N_2 and H_2O [36,66]. Therefore, 6% Ce-2% Sm/CSZ exhibits excellent low-temperature NH_3-SCR performance.

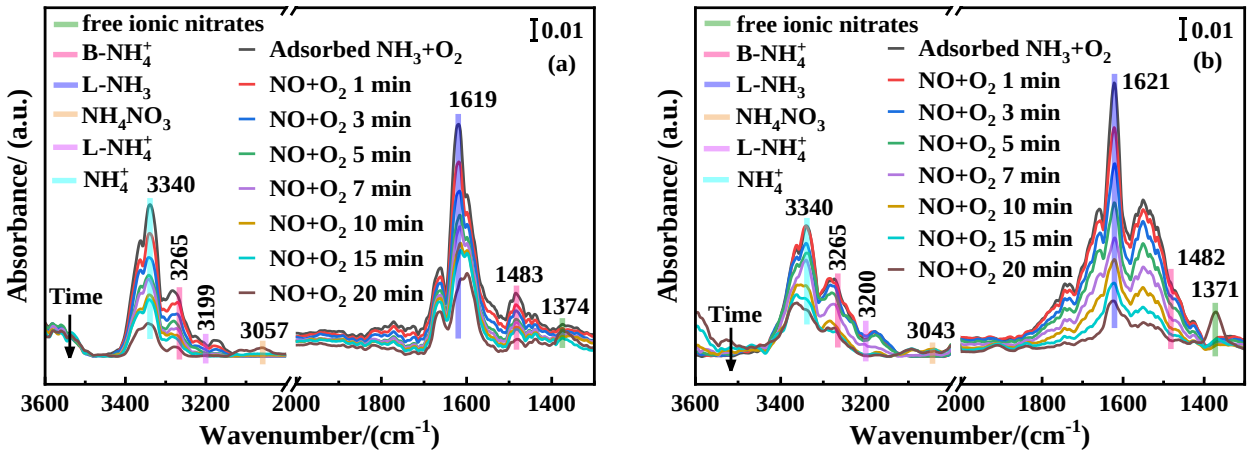

Fig. 11. In situ DRIFTS of pre-adsorbed NH_3 + O_2 followed by reaction with NO + O_2 on (a) 8% Ce/CSZ and (b) 6% Ce-2% Sm/CSZ at 200 ℃.

4. Conclusion

An effective strategy involving the coupling of rare earth oxides (CeO_2 and Sm_2O_3) was employed to enhance the low-temperature NH_3-SCR performance of CSZ. Meanwhile, the coupled CeO_2 and Sm_2O_3 were conducted an in-depth analysis of the synergistic mechanism in the coupled catalysts. 6% Ce-2% Sm/CSZ, as the optimal coupled catalyst, achieves a NOx conversion of 93.1% at 200 ℃ and demonstrates excellent N_2 selectivity in a broad temperature range (100–550 ℃). Additionally, this coupled catalyst also maintains outstanding performance even after exposure to 5 vol% water vapour and thermal aging treatment at 800 °C for 4 h. Physicochemical characterization was performed on the coupled catalysts. The results indicate that crystalline CeO_2 is present on the surface of SSZ-13, while the coupled Sm_2O_3 is extremely uniformly distributed on the surface of SSZ-13 or the introduced Sm_2O_3 is in the nanoscale size. Additional chemisorption oxygen (O_{ads}) provided by coupled CeO_2 is critical for enhancing redox activity. In addition, $[ZCu^{2+}(OH)]^+$ serves as the active sites under low-

temperature conditions, and Sm^{3+} can transfer electrons to $[ZCu^{2+}(OH)]^{+}$ to enhance its activity. The coupled Sm_2O_3 can improve the formation of Ce^{3+} to a certain extent. Additional oxygen vacancies provided by Ce^{3+} can effectively adsorb O_2 in the gas phase and promote the transport of oxygen ions in the coupled catalysts. After coupled CeO_2 and Sm_2O_3, the monodentate nitrates and free ionic nitrates react with gaseous NH_3 via the Eley-Rideal (E-R) route. More importantly, the coupled Sm_2O_3 can generate abundant adsorbed NO_2, which reacts with gaseous NH_3 to participate in the "Fast SCR" reaction. Additionally, the coupled CeO_2 and Sm_2O_3 contain considerable content of both Brønsted and Lewis acid sites on the coupled catalysts, which promote the NH_3 adsorption and facilitate NH_3 activation into NH_4^+. NH_4^+ located at the Brønsted acidic sites can migrate to the Lewis acidic sites. NH_4^+ originating from Lewis acid sites reacts with free ionic nitrates to form NH_4NO_3 via the Langmuir-Hinshelwood (L-H) route. Additionally, the coupled Sm_2O_3 can promote the oxidation of NH_4NO_3 by NO and further form easily decomposable NH_4NO_2. Ultimately, the synergistic effect between Cu species and CeO_2/Sm_2O_3 leads to a substantial boost in low-temperature NH_3-SCR activity of CSZ.

CRediT authorship contribution statement

Ruibin Sun: Writing – original draft, Methodology, Investigation, Data curation, Conceptualization. **Yu Lyu:** Investigation, Methodology. **Chonglin Song:** Writing - review & editing, Project administration, Funding acquisition. **Chenxi Wang:** Investigation, Data curation. **Gang Lyu:** Resources, Formal analysis, Conceptualization. **Xiangyu Dong:** Methodology, Investigation, Data curation. **Lei Tian:** Investigation, Data curation. **Xinhui Liu:** Investigation. **Yibo Xu:** Data curation.

Declare of interest statement

The authors declare that they have no know competing financial interests or personal relationships

that could have appeared to influence the work reported in this paper.

Acknowledgement

This study was supported by the National Natural Science Foundation of China (Grant number: 51921004, 52176123).

Appendix A. Supplementary data

Supplementary data to this article can be found online at XXX.

Reference

[1] Yao L, Liu Q, Mossin S, Nielsen D, Kong M, Jiang L, et al. Promotional effects of nitrogen doping on catalytic performance over manganese-containing semi-coke catalysts for the NH_3-SCR at low temperatures. J Hazard Mater 2020;387:121704. https://doi.org/10.1016/j.jhazmat.2019.121704.

[2] Yang J, Ren S, Zhou Y, Su Z, Yao L, Cao J, et al. In situ IR comparative study on N_2O formation pathways over different valence states manganese oxides c atalysts during NH_3-SCR of NO. Chem Eng J 2020;397:125446. https://doi.org/10.1016/j.cej.2020.125446.

[3] Tang L, Qu J, Mi Z, Bo X, Chang X, Anadon LD, et al. Substantial emission reductions from Chinese power plants after the introduction of ultra-low emissions standards. Nat Energy 2019;4:929–938. https://doi.org/10.1038/s41560-019-0468-1.

[4] Han L, Cai S, Gao M, Hasegawa J, Wang P, Zhang J, et al. Selective catalytic reduction of NOx with NH_3 by using novel catalysts: State of the art and future prospects. Chem Rev 2019;119:10916–10976. https://doi.org/10.1021/acs.chemrev.9b00202.

[5] Feroskhan M, Thangavel V, Subramanian B, Sankaralingam RK, Ismail S, Chaudhary A. Effects of operating parameters on the performance, emission and combustion indices of a biogas fuelled HCCI engine. Fuel 2021;98:120799. https://doi.org/10.1016/j.fuel.2021.120799.

[6] Chen H, Wang X, Pan Z. Effect of operating conditions on the chemical composition, morphology, and nano-structure of particulate emissions in a light hydrocarbon premixed charge compression ignition (PCCI) engine. Sci Total Environ 2021;750:141716. https://doi.org/10.1016/j.scitotenv.2020.141716.

[7] Hariharan D, Krishnan SR, Srinivasan KK, Sohail A. Multiple injection strategies for reducing HC and CO emissions in diesel-methane dual-fuel low temperature combustion. Fuel 2021;305:121372. https://doi.org/10.1016/j.fuel.2021.121372.

[8] Gao N, Geng Z, Zhao W, Geng L, Dong F, Huang D. Review on the combustion and emission characteristics of hydrogen engine. Int J Hydrogen Energy 2025; 143:121–146. https://doi.org/10.1016/j.ijhydene.2025.05.321.

[9] Chen M, Li J, Xue W, Wang S, Han J, Wei Y, et al. Unveiling secondary-ion-promoted catalytic properties of Cu/SSZ-13 zeolites for selective catalytic reduction of NOx. J Am Chem Soc 2022;144:12816–12824. https://doi.org/10.1021/jacs.2c03877.

[10] Han J, Li J, Zhao W, Li L, Chen M, Ge X, et al. Cu-OFF/ERI zeolite: Intergrowth structure synergistically boosting selective catalytic reduction of NOx with NH_3. J Am Chem Soc 2024;146: 7605–7615. https://doi.org/10.1021/jacs.3c13855.

[11] Kim YJ, Kim PS, Kim CH. Deactivation mechanism of Cu/Zeolite SCR catalyst under high-temperature rich operation condition. Appl Catal A Gen 2019;569:175–180. https://doi.org/10.1016/j.apcata.2018.10.032.

[12] Shan Y, Du J, Zhang Y, Shan W, Shi X, Yu Y, et al. Selective catalytic reduction of NOx with NH_3: Opportunities and challenges of Cu-based small-pore zeolites. Natl Sci Rev 2021;8:139–158. https://doi.org/10.1093/nsr/nwab010.

[13] Andana T, Rappé KG, Gao F, Szanyi J, Pereira-Hernandez X, Wang Y. Recent advances in hybrid metal oxide-zeolite catalysts for low-temperature selective catalytic reduction of NOx by ammonia. Appl Catal B Environ 2021;291:120054. https://doi.org/10.1016/j.apcatb.2021.120054.

[14] Beale AM, Gao F, Lezcano-Gonzalez I, Peden CHF, Szanyi J. Recent advances in automotive catalysis for NOx emission control by small-pore microporous materials. Chem Soc Rev 2015;44:7371–7405. https://doi.org/10.1039/C5CS00108K.

[15] Paolucci C, Khurana I, Parekh AA, Li S, Shih AJ, Li H, et al. Dynamic multinuclear sites formed by mobilized copper ions in NOx selective catalytic reduction. Science 2017;357:898–903. https://doi.org/10.1126/science.aan5630.

[16] Paolucci C, Parekh AA, Khurana I, Iorio JRD, Li H, Caballero JDA, et al. Catalysis in a cage: Condition-dependent speciation and dynamics of exchanged Cu cations in SSZ-13 zeolites. J Am Chem Soc 2016;138: 6028–6048. https://doi.org/10.1021/jacs.6b02651.

[17] Wang D, Zhang L, Li J, Kamasamudram K, Epling WS. NH_3-SCR over Cu/SAPO-34-zeolite acidity and Cu structure changes as a function of Cu loading. Catal Today 2014;231:64–74. https://doi.org/10.1016/j.cattod.2013.11.040.

[18] Wang J, Liu J, Tang X, Xing C, Jin T. The promotion effect of niobium on the low-temperature activity of Al-rich Cu-SSZ-13 for selective catalytic reduction of NOx with NH_3. Chem Eng J 2021;418:129433. https://doi.org/10.1016/j.cej.2021.129433.

[19] Lee H, Song I, Jeon SW, Kim DH. Control of the Cu ion species in Cu-SSZ-13 via the introduction of Co^{2+} co-cations to improve the NH_3-SCR activity. Catal Sci Technol 2021;11:4838–4848. https://doi.org/10.1039/D1CY00623A.

[20] Yokoyama C, Misono M. Catalytic reduction of NO by propene in the presence of oxygen over

mechanically mixed metal oxides and Ce-ZSM-5. Catal Lett 1994;29:1–6.

[21] Huang Y, Zhao H, Wu X, Huang Z, Shen H, Jing G. Enhanced low-temperature SCR performance of metal oxide/Cu-SSZ-13 composite catalysts: The role of oxygen species in metal oxide. Chem Eng J 2023;475:146407. https://doi.org/10.1016/j.cej.2023.146407.

[22] Kim HS, Lee H, Park H, Song I, Kim DH. Revealing the two distinctive roles of HY zeolite in enhancing the activity and durability of manganese oxide-zeolite hybrid catalysts for low-temperature NH_3-SCR. Appl Catal B Environ 2024;355:124199. https://doi.org/10.1016/j.apcatb.2024.124199.

[23] Xu S, Li J, Lin Q, Xu H, Wang J, Chen Y. Engineering CeZrOx-Cu/SSZ-13 coupled catalysts to synergistically enhance the low-temperature NH_3-SCR activity. Chem Eng J 2023;476:146767. https://doi.org/10.1016/j.cej.2023.146767.

[24] Kim HS, Lee H, Park H, Song I, Kim DH. Understanding the roles of Brønsted/Lewis acid sites on manganese oxide-zeolite hybrid catalysts for low-temperature NH_3-SCR. Chin J Catal 2024;65:79–88. https://doi.org/10.1016/S1872-2067(24)60112-9.

[25] Deng D, Deng S, He D, Wang Z, Chen Z, Ji Y, et al. A comparative study of hydrothermal aging effect on cerium and lanthanum doped Cu/SSZ-13 catalysts for NH_3-SCR. J Rare Earths 2021;39:969–978. https://doi.org/10.1016/j.jre.2020.08.016.

[26] Lyu Y, Lyu G, Sun R, Song C. Insights into copper-ZSM-5 supported cerium, zirconium catalysts to promote NH_3-SCR activity and anti-thermal aging performance. Fuel 2024;367:131456. https://doi.org/10.1016/j.fuel.2024.131456.

[27] Liu L, Xu K, Su S, He L, Qing M, Chi H, et al Efficient Sm modified Mn/TiO_2 catalysts for selective catalytic reduction of NO with NH_3 at low temperature. Appl Catal A Gen 2020;592:117413. https://doi.org/10.1016/j.apcata.2020.117413.

559 [28] Zhao S, Song K, Jiang R, Ma D, Long H, Shi J. Sm-modified Mn-Ce oxides supported on
560 cordierite as monolithic catalyst for the low-temperature reduction of nitrogen oxides. Catal Today
561 2023;423:113966. https://doi.org/10.1016/j.cattod.2022.11.027.
562 [29] He X, Zhu F, Dong L, Guo H, Liu X, Ren G, et al. Sm-MnOx/TiO_2-{001} with preferentially
563 exposed anatase {001} facet for selective catalytic reduction of NO with NH_3. Appl Catal A Gen
564 2023;644:119353. https://doi.org/10.1016/j.apcata.2023.119353.
565 [30] Wan Y, Yang G, Xiang J, Shen X, Yang D, Chen Y, et al. Promoting effects of water on the NH_3-
566 SCR reaction over Cu-SAPO-34 catalysts: Transient and permanent influences on Cu species. Dalton
567 Trans 2020;49:764–773. https://doi.org/10.1039/C9DT03848E.
568 [31] Gao F, Mei D, Wang Y, Szanyi J, Peden CHF. Selective catalytic reduction over Cu/SSZ-13:
569 Linking homo- and heterogeneous catalysis. J Am Chem Soc 2017;139:4935–4942.
570 https://doi.org/10.1021/jacs.7b01128.
571 [32] Wang D, Zhang L, Kamasamudram K, Epling WS. In Situ-DRIFTS study of selective catalytic
572 reduction of NOx by NH_3 over Cu-exchanged SAPO-34. ACS Catal 2013;3:871–881.
573 https://doi.org/10.1021/cs300843k.
574 [33] Yu T, Wang J, Shen M, Wang J, Li W. The influence of CO_2 and H_2O on selective catalytic
575 reduction of NO by NH_3 over Cu/SAPO-34 catalyst. Chem Eng J 2015;264:845–855.
576 https://doi.org/10.1016/j.cej.2014.12.017.
577 [34] Shan Y, Shan W, Shi X, Du J, Yu Y, He H. A comparative study of the activity and hydrothermal
578 stability of Al-rich Cu-SSZ-39 and Cu-SSZ-13. Appl Catal B Environ 2020;264:118511.
579 https://doi.org/10.1016/j.apcatb.2019.118511.
580 [35] Chen M, Wei Y, Han J, Yan W, Yu J. Enhancing catalytic performance of Cu-SSZ-13 for the

581 NH_3-SCR reaction via in situ introduction of Fe^{3+} with diatomite. Mater Chem Front 2021;5:7787–
582 7795. https://doi.org/10.1039/D1QM01101D.
583 [36] Liu Q, Fu Z, Ma L, Niu H, Liu C, Li J, et al. MnOx-CeO_2 supported on Cu-SSZ-13: A novel SCR
584 catalyst in a wide temperature range. Appl Catal A Gen 2017;547:146–154.
585 https://doi.org/10.1016/j.apcata.2017.08.024.
586 [37] Tong Y, Li Y, Li Z, Wang P, Zhang Z, Zhao X, et al. Influence of Sm on the low temperature
587 NH_3-SCR of NO activity and H_2O/SO_2 resistance over the $Sm_aMnNi_2Ti_7O_x$ (a = 0.1, 0.2, 0.3, 0.4)
588 catalysts. Appl Catal A Gen 2020;590:117333. https://doi.org/10.1016/j.apcata.2019.117333.
589 [38] Xie M, Xiao X, Wang J, Chen J, Kang H, Wang N, et al. Mechanistic insights into the cobalt
590 promotion on low-temperature NH_3-SCR reactivity of Cu/SSZ-13. Sep Purif Technol
591 2023;315:123617. https://doi.org/10.1016/j.seppur.2023.123617.
592 [39] Chen M, Zhao W, Wei Y, Han J, Li J, Sun C, et al. La ions-enhanced NH_3-SCR performance over
593 Cu-SSZ-13 catalysts. Nano Res 2023;16:12126–12133. https://doi.org/10.1007/s12274-023-5500-x.
594 [40] Song J, Wang Y, Walter ED, Washton NM, Mei D, Kovarik L, et al. Toward rational design of
595 Cu/SSZ-13 selective catalytic reduction catalysts: Implications from atomic-level understanding of
596 hydrothermal stability. ACS Catal 2017;7:8214–8227. https://doi.org/10.1021/acscatal.7b03020.
597 [41] Fan C, Chen Z, Pang L, Ming S, Dong C, Albert KB, et al. Steam and alkali resistant Cu-SSZ-13
598 catalyst for the selective catalytic reduction of NOx in diesel exhaust. Chem Eng J 2018;334:344–354.
599 https://doi.org/10.1016/j.cej.2017.09.181.
600 [42] Wang X, Xu Y, Qin M, Zhao Z, Fan X, Li Q. Insight into the effects of Cu^{2+} ions and CuO species
601 in Cu-SSZ-13 catalysts for selective catalytic reduction of NO by NH_3. J Colloid Interface Sci
602 2022;622:1–10. https://doi.org/10.1016/j.jcis.2022.04.110.

603 [43] Niu C, Shi X, Liu F, Liu K, Xie L, You Y, et al. High hydrothermal stability of Cu-SAPO-34
604 catalysts for the NH_3-SCR of NOx. Chem Eng J 2016;294:254–263.
605 https://doi.org/10.1016/j.cej.2016.02.086.
606 [44] Liu J, Du Y, Liu J, Zhao Z, Cheng K, Chen Y, et al. Design of MoFe/Beta@CeO_2 catalysts with
607 a core-shell structure and their catalytic performances for the selective catalytic reduction of NO with
608 NH_3. Appl Catal B Environ 2017;203:704–714. https://doi.org/10.1016/j.apcatb.2016.10.039.
609 [45] Chang H, Chen X, Li J, Ma L, Wang C, Liu C, et al. Improvement of activity and SO_2 tolerance
610 of Sn-modified MnOx-CeO_2 catalysts for NH_3-SCR at low temperatures. Environ Sci Technol
611 2013;47:5294–5301. https://doi.org/10.1021/es304732h.
612 [46] Shi Y, Pu J, Gao L, Shan S. Selective catalytic reduction of NOx with NH_3 and CH_4 over zeolite
613 supported indium-cerium bimetallic catalysts for lean-burn natural gas engines. Chem Eng J
614 2021;403:126394. https://doi.org/10.1016/j.cej.2020.126394.
615 [47] Chen L, Wang X, Cong Q, Ma H, Li S, Li W. Design of a hierarchical Fe-ZSM-5@CeO_2 catalyst
616 and the enhanced performances for the selective catalytic reduction of NO with NH_3. Chem Eng J
617 2019; 369:957–967. https://doi.org/10.1016/j.cej.2019.03.055.
618 [48] Chen J, Fu P, Lv D, Chen Y, Fan M, Wu J, et al. Unusual positive effect of SO_2 on Mn-Ce mixed-
619 oxide catalyst for the SCR reaction of NOx with NH_3. Chem Eng J 2021;407:127071.
620 https://doi.org/10.1016/j.cej.2020.127071.
621 [49] Liu C, Chen L, Li J, Ma L, Arandiyan H, Du Y, et al. Enhancement of activity and sulfur resistance
622 of CeO_2 supported onTiO_2-SiO_2 for the selective catalytic reduction of NO by NH_3. Environ Sci
623 Technol 2012;46:6182–6189. https://doi.org/10.1021/es3001773.
624 [50] Liu H, Fan Z, Sun C, Yu S, Feng S, Chen W, et al. Improved activity and significant SO_2 tolerance

625 of samarium modified CeO_2-TiO_2 catalyst for NO selective catalytic reduction with NH_3. Appl Catal
626 B Environ 2019;244:671–683. https://doi.org/10.1016/j.apcatb.2018.12.001.
627 [51] Sun C, Liu H, Chen W, Chen D, Yu S, Liu A, et al. Insights into the Sm/Zr co-doping effects on
628 N_2 selectivity and SO_2 resistance of a MnOx-TiO_2 catalyst for the NH_3-SCR reaction. Chem Eng J
629 2018;347:27–40. https://doi.org/10.1016/j.cej.2018.04.029.
630 [52] Yu JJ, Jiang Z, Zhu L, Hao ZP, Xu ZP. Adsorption/Desorption studies of NOx on well-mixed
631 oxides derived from Co-Mg/Al hydrotalcite-like compounds. J Phys Chem B 2006;110:4291–4300.
632 https://doi.org/10.1021/jp056473f.
633 [53] Li B, Song C, Lv G, Chen K, Cao X. Impact of soot on NOx adsorption over Cu-modified
634 hydrotalcite-derived lean NOx trap catalyst. Langmuir 2017;33:2939–2948.
635 https://doi.org/10.1021/acs.langmuir.6b03877.
636 [54] Kubota H, Liu C, Toyao T, Maeno Z, Ogura M, Nakazawa N, et al. Formation and reactions of
637 NH_4NO_3 during transient and steady-state NH_3-SCR of NOx over H-AFX zeolites: Spectroscopic and
638 theoretical studies. ACS Catal 2020;10:2334–2344. https://doi.org/10.1021/acscatal.9b05151.
639 [55] Wang Y, Li G, Zhang S, Zhang X, Zhang X, Hao Z. Promoting effect of Ce and Mn addition on
640 Cu-SSZ-39 zeolites for NH_3-SCR reaction: Activity, hydrothermal stability, and mechanism study.
641 Chem Eng J 2020;393:124782. https://doi.org/10.1016/j.cej.2020.124782.
642 [56] Wang X, Li T, Wang C, Cui Q, Wang T, Bao X, et al. Improving catalytic performance of Cu-
643 SSZ-13 for NOx abatement via in-situ introduction of La and Ce from spent catalyst. Sep Purif Technol
644 2024;331:125638. https://doi.org/10.1016/j.seppur.2023.125638.
645 [57] Xu Q, Fang Z, Chen Y, Guo Y, Guo Y, Wang L, et al. Titania-samarium-manganese composite
646 oxide for the low-temperature selective catalytic reduction of NO with NH_3. Environ Sci Technol

2020;54:2530–2538. https://dx.doi.org/10.1021/acs.est.9b06701.

[58] Gao F, Washton NM, Wang Y, Kollár M, Szanyi J, Peden CHF. Effects of Si/Al ratio on Cu/SSZ-13 NH_3-SCR catalysts: Implications for the active Cu species and the roles of Brønsted acidity. J Catal 2015;331:25–38. https://doi.org/10.1016/j.jcat.2015.08.004.

[59] Han S, Cheng J, Zheng C, Ye Q, Cheng S, Kang T, et al. Effect of Si/Al ratio on catalytic performance of hydrothermally aged Cu-SSZ-13 for the NH_3-SCR of NO in simulated diesel exhaust. Appl Surf Sci 2017;419:382–392. https://doi.org/10.1016/j.apsusc.2017.04.198.

[60] Luo J, Wang D, Kumar A, Li J, Kamasamudram K, Currier N, et al. Identification of two types of Cu sites in Cu/SSZ-13 and their unique responses to hydrothermal aging and sulfur poisoning. Catal Today 2016;267:3–9. https://doi.org/10.1016/j.cattod.2015.12.002.

[61] Wang D, Jangjou Y, Liu Y, Sharma MK, Luo J, Li J, et al. A comparison of hydrothermal aging effects on NH_3-SCR of NOx over Cu-SSZ-13 and Cu-SAPO-34 catalysts. Appl Catal B Environ 2015;165:438–445. https://doi.org/10.1016/j.apcatb.2014.10.020.

[62] Wang B, Feng X, Xu Y, Shi J. Role of Ce in promoting low-temperature performance and hydrothermal stability of Ce/Cu-SSZ-13 in the selective catalytic reduction of NOx with NH_3. Sep Purif Technol 2023;315:123679. https://doi.org/10.1016/j.seppur.2023.123679.

[63] Xu M, Wang J, Yu T, Wang J, Shen M. New insight into Cu/SAPO-34 preparation procedure: Impact of NH_4-SAPO-34 on the structure and Cu distribution in Cu-SAPO-34 NH_3-SCR catalysts. Appl Catal B Environ 2018;220:161–170. https://doi.org/10.1016/j.apcatb.2017.08.031.

[64] Zhao Z, Yu R, Shi C, Gies H, Xiao F, Vos DD, et al. Rare-earth ion exchanged Cu-SSZ-13 zeolite from organotemplate-free synthesis with enhanced hydrothermal stability in NH_3-SCR of NOx. Catal Sci Technol 2019;9:241–251. https://doi.org/10.1039/C8CY02033G.

669 [65] Wang Y, Shi X, Shan Y, Du J, Liu K, He H. Hydrothermal stability enhancement of Al-rich Cu-
670 SSZ-13 for NH_3 selective catalytic reduction reaction by ion exchange with cerium and samarium. Ind
671 Eng Chem Res 2020;59:6416–6423. https://doi.org/10.1021/acs.iecr.0c00285.
672 [66] Su W, Chang H, Peng Y, Zhang C, Li J. Reaction pathway investigation on the selective catalytic
673 reduction of NO with NH_3 over Cu/SSZ-13 at low temperatures. Environ Sci Technol 2015;49:467–
674 473. https://doi.org/10.1021/es503430w.